Determining Waveguide Group Index Based On Measurement of MZI Gain Spectrum

Jeff DiMaria (EdX Username: Dangerzone)

***Abstract*— This study shows that the group index of a waveguide can be determined accurately from the gain spectrum of a Mach-Zehnder Interferometer (MZI) photonic integrated circuit. The path length difference between the arms of the MZI is varied to determine the range over which the MZI can be used to accurately assess the group index of the waveguide.**

I. INTRODUCTION

Mach-Zehnder interferometers (MZIs) are a class of optical interferometers where light is split into two different paths whose output intensity varies based upon the phase difference accrued when the light recombines at the output ports. This phase difference depends on a several factors including the refractive index of the waveguide and the geometric length of each arm. The goal of this study is to determine the group index (n_g) of the first supported quasi-TE mode of Si waveguide of a given geometric cross section by measuring the gain spectrum for devices with different MZI path length differences.

II. THEORY

The group index (n_g) can be calculated from the effective index (n_{eff}) of the waveguide mode from Equation 1:

$$n_g(\lambda) = n_{eff}(\lambda) - \lambda \cdot \frac{\partial n_{eff}(\lambda)}{\partial \lambda} \quad (1)$$

In practice this cannot be directly measured, but can be determined from the phase differences of light through an MZI component. A diagram of the MZI based upon two Y-branches is shown in Figure 1.

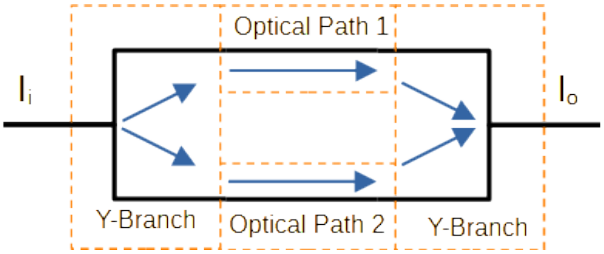

Figure 1: Basic MZI Diagram

The intensity transfer function relating the intensity measured at the output port relative to that on the input port is:

$$I_o = \frac{Ii}{2} \cdot \left(1 + \cos(\beta \Delta L)\right) \quad (2)$$

Where $\beta = 2\pi n_{eff} / \lambda$ and ΔL is the geometric path length difference between each branch of the MZI.
The sinusoidal modulation of the intensity profile is determined based upon the interference caused by the phase difference of the electromagnetic waves propagating down each arm of the spectrometer. The spacing between interference maximum, i.e. the free spectral range, is related to the group index by:

$$FSR(\lambda) = \frac{\lambda^2}{\Delta L \cdot n_g(\lambda)} \quad (3)$$

By fitting the effective index to the gain spectra for MZI with different ΔL near 1.55um, n_g of the waveguide can be determined based upon Equation 2. The FSR can be used to validate the model and fit.

III. MODELING AND SIMULATION

The analysis begins with a simulation of the supported modes of the waveguide with Lumerical MODE. The waveguide is modeled as a 220nm x 500nm cross-section with a semi-infinite Si core and SiO2 cladding. The simulation boundary is perfectly-matched layer on all 4 sides with XY dimensions 2.5um x 1.7um as shown in Figure 2.

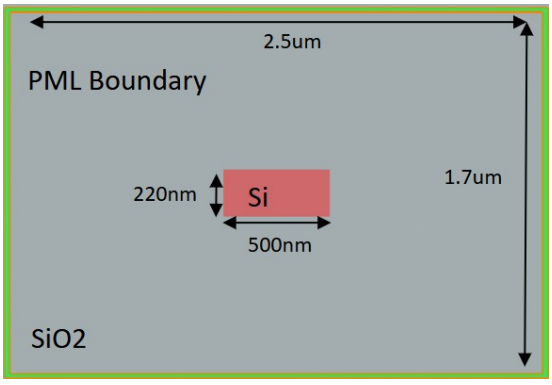

Figure 2: Modeled Waveguide Cross Section

The focus of this analysis is on the first-supported quasi-TE mode at 1.55um wavelength. This mode's E-field intensity profile is shown in Figure 3.

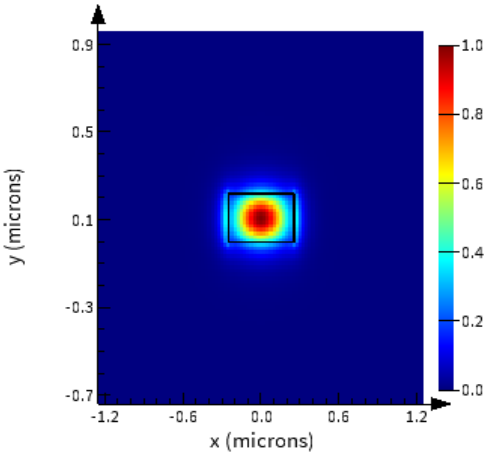

Figure 3: First quasi-TE E-field intensity profile at λ=1.55um

The effective index of the waveguide mode is extracted from Lumerical MODE solver and a Taylor expansion fit to these results is determined between 1.5um and 1.6um according to Equations 4 and 5.

$$n_{eff}(\lambda) = n_{eff\,1} + n_{eff\,2}(\lambda - 1.55\,\mu m) + n_{eff\,3}(\lambda - 1.55\,\mu m)^2 \quad (4)$$

$$n_{eff}(\lambda) = 2.447 + 1.134(\lambda - 1.55\,\mu m) - 0.041(\lambda - 1.55\,\mu m)^2 \quad (5)$$

The n_{eff} vs. λ is shown in Figure 4.

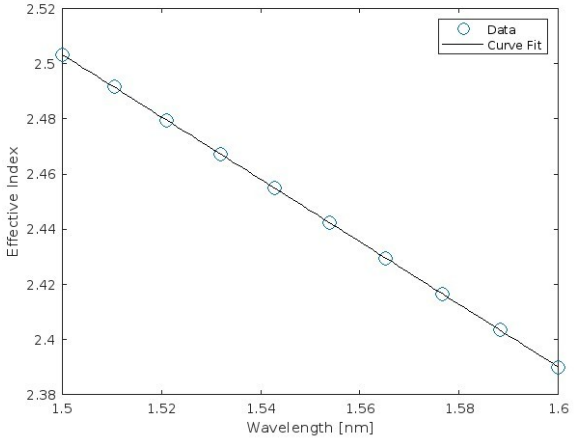

Figure 4: Modeled Effective index vs. Wavelength

The group index for this Si waveguide is also calculated by the software and is plotted in Figure 5 for different wavelengths.

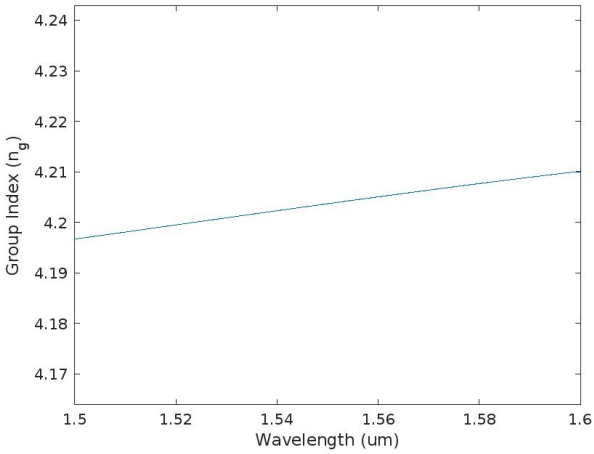

Figure 5: Modeled Group Index vs. Wavelength

In order to experimentally determine the group index via Equation 2, a series of MZI designs is proposed. The study focuses on a modification of the design in Figure 6.

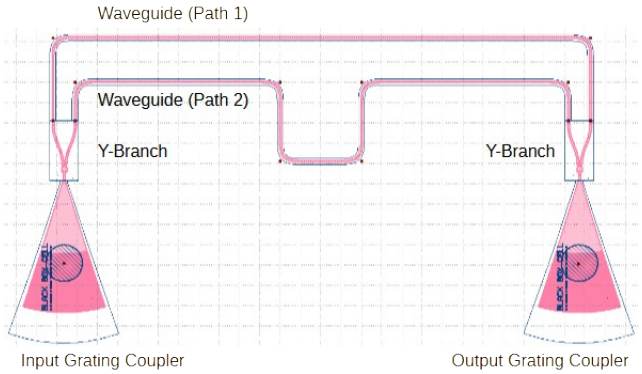

Figure 6: Example MZI Layout Including Grating Couplers

Laser light is coupled into the MZI via a fiber and input grating coupler. The light is then split via a Y-branch into 2 waveguide paths (#1 and #2). The supported mode propagates through each path, recombines at the second Y-branch, and is outcoupled to a fiber and optical spectrum analyzer. In this study waveguide path #2 is increased from the balanced case (ΔL=0um) through various unbalanced cases. Table 1 contains the path length differences considered in this study. A simple waveguide without MZI and a balanced MZI where the two waveguide paths are equivalent are added as controls to check waveguide losses and assess fabrication tolerances.

Design	MZI ΔL (μm)	FSR (nm)
Straight WG	N.A.	N.A.
MZI 1	0	N.A.
MZI 2	25	21.4
MZI 3	35	15.6
MZI 4	45	12.5
MZI 5	55	10.2
MZI 6	65	8.9
MZI 7	75	7.4
MZI 8	85	6.8
MZI 9	95	6

Table 1 - Design ΔL and Calculated FSR

The optical gain of each circuit is simulated in Lumerical INTERCONNECT and an example of the gain spectra are plotted in Figure 7 for the balanced MZI (ΔL = 0um) and MZI 9 (ΔL=95um).

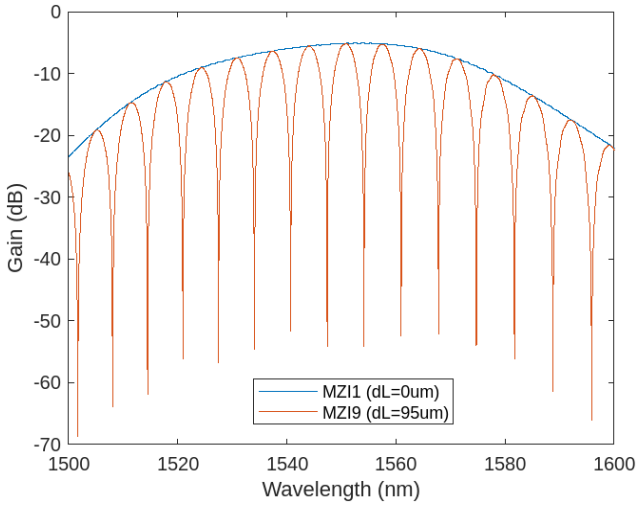

Figure 7: Example of modeled optical gain for MZI with ΔL = 0um and 95um

The FSR is determined by finding the wavelength difference between peaks nearest to 1.55um wavelength. The modeled FSR is listed in Table 1 and shown in Figure 8.

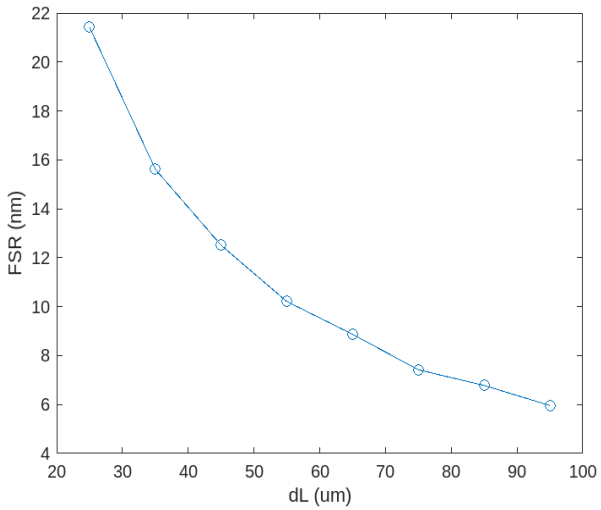

Figure 8: Modeled FSR for MZIs with different ΔL

A corner analysis was conducted for the expected process variation with process center at 220nm waveguide thickness and 500nm waveguide width. The waveguide thickness was expected to vary between 215nm to 223nm and waveguide width expected to vary between 470nm and 510nm. The expected variation in group index is shown in Figure 9. The group index decreases as waveguide width and thickness increase.

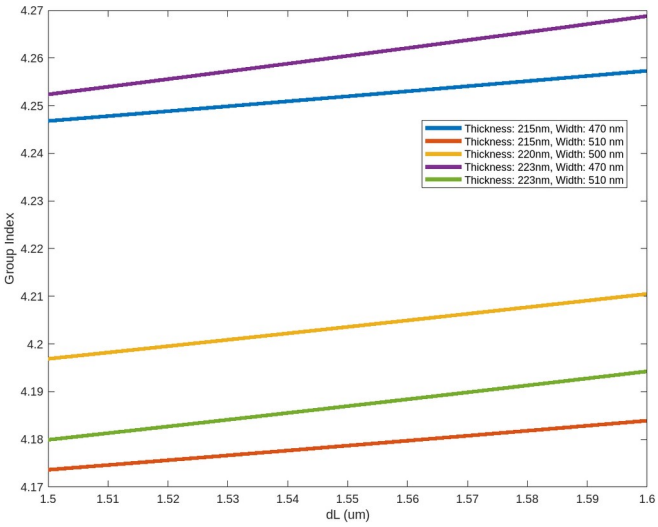

Figure 9: Corner Analysis of Group Index Due to Waveguide Width and Height Variation

The expected variation in effective index is shown in Figure 10. The effective index increases as waveguide width and thickness increase and decreases as waveguide width and thickness decrease. This relationship is more strongly dependent on thickness variation than width variation as evidenced by 215nm x 510nm having lower effective index

than 220nm x 500nm despite the waveguide being narrower in this case.

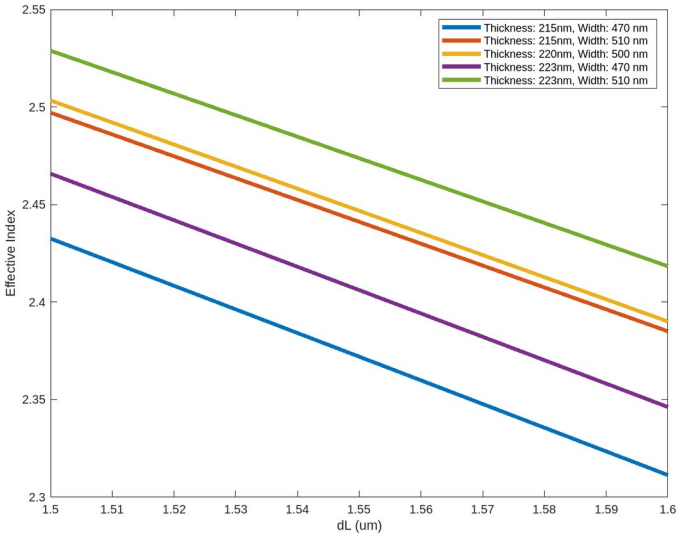

Figure 10: Corner Analysis of Effective Index Due to Waveguide Width and Height Variation

The expected variation in FSR due to variations in waveguide width and thickness for each design are shown in Table 2. The variation is larger for smaller path length differences (MZI 2) than larger path length differences (MZI 9).

Design	MZI ΔL (μm)	FSR min (nm)	FSR max (nm)
Straight WG	N.A.	N.A.	N.A.
MZI 1	0	N.A.	N.A.
MZI 2	25	21.4	23.2
MZI 3	35	15.6	16.4
MZI 4	45	12.5	12.7
MZI 5	55	10.2	10.4
MZI 6	65	8.9	8.9
MZI 7	75	7.4	7.7
MZI 8	85	6.8	6.8
MZI 9	95	6	6.1

Table 2: MZI ΔL and Calculated FSR min and max due to Waveguide Thickness and Width Variation.

IV. FABRICATION

The devices defined in Table 1 were submitted for fabrication at Applied Nanotools. Silicon-on-insulator wafers with 200mm diameter, 220nm silicon device layer thickness, and 2um buffer oxide were used as a template. Devices were diced into 25x25mm chips, cleaned in piranha solution of 3:1 H2SO4:H2O2) for 15 minutes then rinsed in IPA/DI water. The substrate was coated with HSQ resist followed by hard-bake. The resist was patterned via e-beam lithography and developed with TMAH. The devices then underwent patterning of the silicon layer via Cl-based anisotropic ICP-RIE. The resist was subsequently removed via 10:1 BOE and a 2.2um oxide cladding layer was deposited via PECVD and TEOS recipe at 300 C. An example plan-view SEM of other devices fabricated in this run is shown in Figure 11 (note: SEM images of devices in this report were not requested or taken).

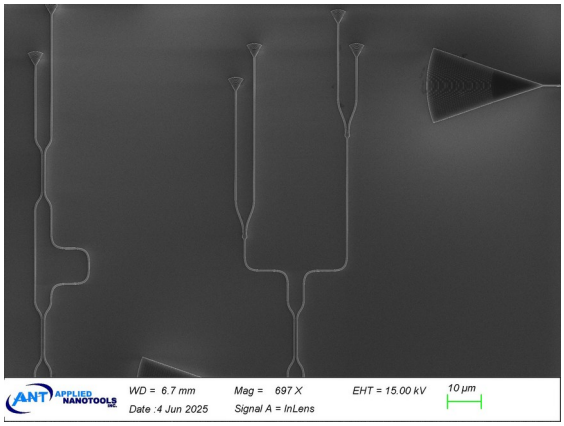

Figure 11: Example plan-view of other devices fabricated in same production run.

V. EXPERIMENTAL DATA

To characterize the devices, a custom-built automated test setup [1, 5] with automated control software written in Python was used [2]. An Agilent 81600B tunable laser was used as the input source and Agilent 81635A optical power sensors as the output detectors. The wavelength was swept from 1500 to 1600 nm in 10 pm steps. A polarization maintaining (PM) fibre was used to maintain the polarization state of the light, to couple the TE polarization into the grating couplers [3]. A polarization maintaining fibre array was used to couple light in/out of the chip [4].

An example of the measured gain of one of the MZI devices is shown in Figure 12. All other devices were characterized similarly.

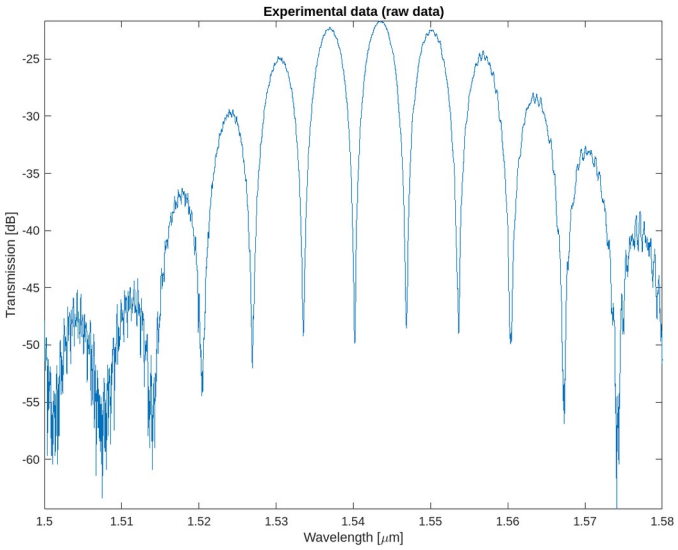

Figure 12: Example of measured gain spectrum (MZI8).

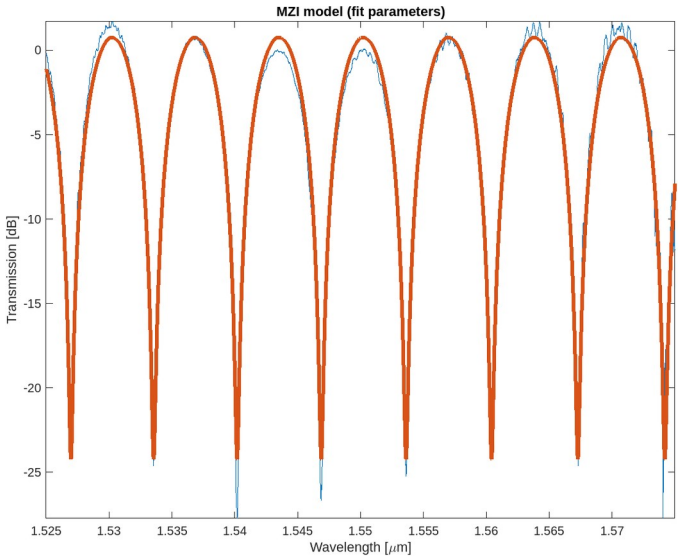

Figure 13: MZI8 model gain after fitting to account for variations in process parameters.

VI. ANALYSIS

In order to extract the group index for the waveguide, the gain spectra were first estimated based on a theoretical model of MZI performance. The theoretical model assumes a nominal ΔL and waveguide effective index as a starting point. Due to deviations in effective index caused by process variation in the experimental devices, the MZI gain spectra will be shifted relative to the initial theoretical expectation. First, the gain spectra are first baseline corrected to account for grating coupler loss spectral efficiency variation. To account for process variations in waveguide width and thickness the model effective index is fit to closely match the measured spectral features for each ΔL. An example of the MZI model gain spectrum before and after baseline correction and fitting are shown in Figures 12 and 13. In the latter case the spectral region of interest was truncated between 1.525um and 1.575um in order to avoid fitting to noise <1.52um and >1.575um.

The group index for each MZI was subsequently determined based upon the effective index that most closely matched the experimental data after applying Equation (1). An example of the extracted group index vs. wavelength for MZI8 is shown in Figure 14.

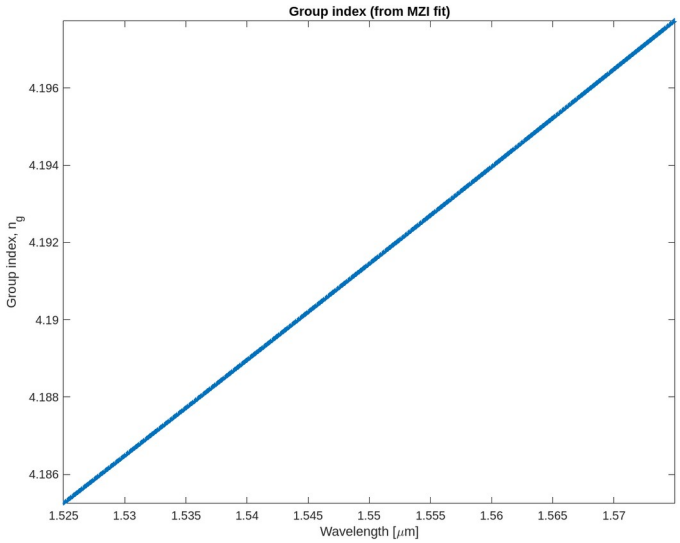

Figure 14: Extracted group index for MZI8 based on best-fit effective index.

All other MZI designs were fit accordingly and the experimental vs. simulated group indices at 1.55um are shown in Table 3.

Design	MZI ΔL (μm)	Model FSR (nm)	Experimental FSR (nm)	Group Index (ng)
MZI 2	25	21.4	23.4	Poor Fit
MZI 3	35	15.6	16.6	4.173
MZI 4	45	12.5	12.7	4.191
MZI 5	55	10.2	10.3	4.189
MZI 6	65	8.9	8.8	4.192
MZI 7	75	7.4	7.7	4.189
MZI 8	85	6.8	6.8	4.191
MZI 9	95	6	6	4.187
			Average:	4.187

Table 3: FSR and extracted waveguide group index for each MZI configuration.

Plot of FSRs near 1.55um for different ΔL configurations are shown in Figure 15.

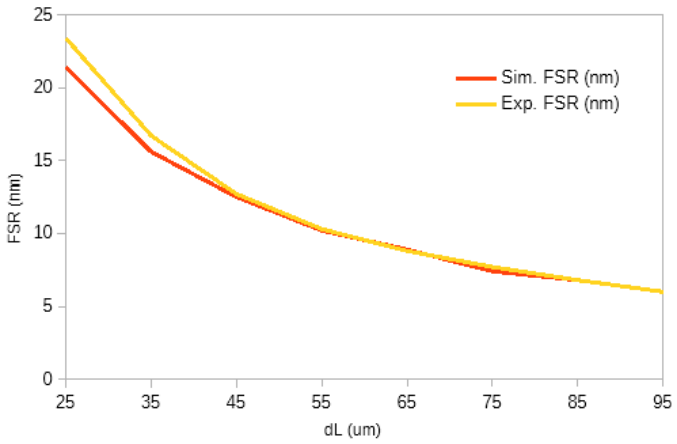

Figure 15: Simulated vs. Experimental FSR for different ΔL

For most MZI configurations, particularly ΔL>25um, the group index variation is relatively small (+/- 0.5%) and the agreement between initially modeled FSR and experimental FSR is quite low (<1nm). For MZI2, the experimental FSR deviated from the model and the group index was unable to be fit due to having too few noise-free spectral features in the wavelength range of interest. The average group index for the waveguide in this study based upon extraction from fitting to different MZI gain spectra is 4.187, which is about 3% lower than the initial modeling estimate (ng~4.2) based upon nominal material properties and ideal waveguide dimensions. This indicates that the waveguides fabricated in this study are likely somewhat wider than the nominal value of 500nm, but within the process variability upper limit of 510nm as considered in the corner analysis.

VII. CONCLUSIONS

This study explored utilizing the gain spectra of different MZI devices to determine the group index of the first supported quasi-TE mode of a SOI waveguide with 220nm x 500nm nominal dimensions. The MZIs in this study have been proven to be sufficient to extract the average group index ~4.187 for this waveguide with sufficient precision. It is noted that MZI path length >25um is critical to ensure sufficient precision and accuracy of the extraction methodology employed in this study.

REFERENCES

[1] Lukas Chrostowski, Michael Hochberg, chapter 12 in "Silicon Photonics Design: From Devices to Systems", Cambridge University Press, 2015

[2] http://siepic.ubc.ca/probestation, using Python code developed by Michael Caverley.

[3] Yun Wang, Xu Wang, Jonas Flueckiger, Han Yun, Wei Shi, Richard Bojko, Nicolas A. F. Jaeger, Lukas Chrostowski, "Focusing sub-wavelength grating couplers with low back reflections for rapid prototyping of silicon photonic circuits", Optics Express Vol. 22, Issue 17, pp. 20652-20662 (2014) doi: 10.1364/OE.22.020652

[4] www.plcconnections.com, PLC Connections, Columbus OH, USA.

[5] http://mapleleafphotonics.com, Maple Leaf Photonics, Seattle WA, USA.